Tunable magnetism of a hexagonal Anderson droplet on the triangular lattice

Mi Jiang
Stewart Blusson Quantum Matter Institute, University of British Columbia, Vancouver, British Columbia, Canada

(Received 27 March 2019; revised manuscript received 13 June 2019; published 19 July 2019)

Motivated by recent progress on quantum engineered Kondo lattices, we numerically investigated the local magnetic properties of a hexagonal Anderson droplet consisting of multiple rings of magnetic atoms periodically arrayed on a triangular lattice. We demonstrated the tunability of the magnetic properties via their evolution with the droplet geometry for two types of systems with distinct local orbital occupancy profiles. We found that the local susceptibility of the droplet center of some types of droplets can be remarkably enhanced, in contrast to the conventionally rapid decrease due to spin correlations of surrounding droplet rings. The tunability of the magnetic properties is attributed to the charge redistribution with varying the droplet geometry enforced by the confined lattice with an open boundary. Our simulations complement the exploration of the novel artificial tunability of engineered lattice systems.

DOI: 10.1103/PhysRevB.100.014422

I. INTRODUCTION

There has been a recent paradigm shift in the investigation of strongly correlated electronic systems from real materials to the atomic-scale manipulation of artificial lattices and/or superlattices [1–8]. For example, in the context of the Kondo physics in heavy-fermion materials [9], the realization of artificial lattices has provided a radically new platform to both explore and manipulate the emergence of strong correlation effects. The resulting many-body phenomena at the nanoscale permit the diverse opportunities for studying the interplay between different degrees of freedom in a controllable manner. In particular, the quantum engineering of nanoscopic Kondo droplets has been demonstrated to be capable of coherently controlling the droplet's properties such as its Kondo temperature [1]. Theoretically, they employed large-N expansion for the treatment of the triangular Cu(111) surface lattice, which allows for two types of hexagonal magnetic atom droplets. This study demonstrated the possibility of not only creating coherently coupled Kondo droplets but also modifying the droplet's Kondo temperature via changing a droplet's real-space geometry. As a closely related aspect of the Kondo droplets, the requisite conditions of the coherent Kondo lattice behavior for periodically arranged magnetic moments on a square lattice within the particle-hole symmetric Kondo lattice model (KLM) was investigated as well recently [10].

It is well known that another type of model that is believed to qualitatively describe the essential features of the rich physics of heavy-fermion systems is the Anderson model, e.g., the single-impurity or periodic Anderson model, whose relation to the Kondo models has been extensively explored in recent decades [11,12]. As effective models in the strong-coupling limit, Kondo models describe the f electrons as localized quantum-mechanical spins so that the charge degrees of freedom can be discarded. Hence, given the recent experimental progress on realizing atomic-scale manipulation of artificial lattices and the theoretical exploration of Kondo droplets [1], it is a good moment to thoroughly investigate the properties of the hexagonal Anderson droplet with the additional involvement of the charge degrees of freedom.

Here we numerically explore the local magnetic properties of a hexagonal Anderson droplet consisting of multiple rings of magnetic atoms on a triangular lattice in the framework of the Anderson model, which has richer physics than its counterpart Kondo model because of the intrinsic charge fluctuations of f electrons. Our focus is the evolution of the local properties within the droplet and, more importantly, their dependence on the spatial structure of the droplet.

This paper is organized as follows. In Sec. II, we define our Anderson droplet model and the determinant quantum Monte Carlo method employed. Section III discusses the local magnetic susceptibilities and closely related density modulations in various droplets. Section IV illustrates more evidence of the dependence of magnetic properties on various parameters. The summary and future issues to be addressed are presented in Sec. V.

II. MODELS AND METHODS

We employ the two-dimensional Anderson droplet model (ADM) in the half-filled form on a triangular lattice

$$\mathcal{H} = -t\sum_{\langle ij\rangle,\sigma}(c^{\dagger}_{i\sigma}c_{j\sigma}+c^{\dagger}_{j\sigma}c_{i\sigma}) - V\sum_{i\in D,\sigma}(c^{\dagger}_{i\sigma}f_{i\sigma}+f^{\dagger}_{i\sigma}c_{i\sigma}) + U\sum_{i\in D}\left(n^{f}_{i\uparrow}-\frac{1}{2}\right)\left(n^{f}_{i\downarrow}-\frac{1}{2}\right) - \mu\left(\sum_{i\sigma}n^{c}_{i\sigma}+\sum_{i\in D,\sigma}n^{f}_{i\sigma}\right),$$

where $c^{\dagger}_{i\sigma}$ ($c_{i\sigma}$) and $f^{\dagger}_{i\sigma}$ ($f_{i\sigma}$) are creation (annihilation) operators for the conduction and local f electrons on site i with spin σ, respectively. $n^{c,f}_{i\sigma}$ are the associated number operators. $t = 1$, set to be the energy unit, is the hopping amplitude between conduction electrons on nearest-neighbor sites $\langle ij\rangle$ of a triangular lattice. U denotes the local repulsive interaction for f electrons, and V is the hybridization between the conduction and f electrons. The chemical potential μ

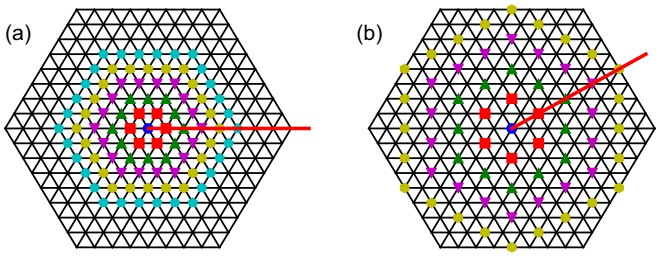

FIG. 1. Lattice structure of two types of Anderson droplets consisting of multiplet rings of Anderson impurities with distance (a) na_0 and (b) $\sqrt{3}na_0$, with $a_0 \equiv 1$ being the lattice constant. n is an integer, and only the $n = 1$ case is shown here. The red line denotes the direction adopted to examine the evolution of local properties.

controls the average density of the system. The set D defines the set of sites where the impurity droplet resides. Figure 1 illustrates the geometrical structure of our hexagonal lattice with an open boundary and two types of droplets, where the distance between the consecutive impurity rings can be na_0 and $\sqrt{3}na_0$ separately, with $a_0 \equiv 1$ being the lattice constant and n being an integer. This geometry has direct relevance to a recent study on the artificially engineered Kondo droplet system [1]. From now on, we denote the spatial structure of the droplet by $A/B\{n : N_r\}$, with n being the distance between consecutive rings and N_r being the number of rings such that Fig. 1 shows $A\{1 : 5\}$ and $B\{1 : 4\}$ droplets. With this notation, for example, the first ring of the $A\{3 : 2\}$ droplet has the same location as the third ring of the $A\{1 : 4\}$ droplet.

Although the ADM model breaks the translational symmetry of the lattice, it has a close relation to the well-known periodic Anderson model (PAM), which is conventionally believed to capture the essential physics of heavy-fermion materials [9]. Accordingly, the PAM has been extensively explored numerically in various contexts, for example, the phase diagram [13,14], the universal Knight shift anomaly [15], d-wave superconductivity [16], the Mott metal-insulator transition [17–19], etc. The ADM can also be viewed as a special form of the depleted PAM [20] and is relevant to the PAM with impurities [21,22].

The phase diagram of the PAM on a triangular lattice, which hosts richer phases than its counterpart on a square lattice, has been explored extensively in recent decades [23,24]. Following the phase diagram reported in [23], we focus on the characteristic intermediate-coupling strength $U/t = 4.0$ and $c - f$ hybridization strength $V/t = 1.0$ such that they are the same order of magnitude. More detailed dependence on the parameters such as U and V will be addressed in Sec. IV. To treat with these energy scales on equal footing, we solve the ADM by means of the conventional finite-temperature determinant Quantum Monte Carlo (DQMC) [25]. Note that our hexagonal-shaped triangular lattice with an open boundary is highly inhomogeneous and nonperiodic, so that both the conduction and f electron density distributions will affect the local properties throughout the lattice. As discussed below, this inhomogeneity of density fluctuations is believed to be decisive in the determination of the local magnetic properties. In this work, we have treated two characteristic types of systems: (i) the whole system is half filled, $\rho = [\sum_{i\sigma}\langle n^c_{i\sigma}\rangle + \sum_{i\in D,\sigma}\langle n^f_{i\sigma}\rangle]/N = 1$, with N being the total number of lattice sites (including the droplet), by tuning the chemical potential μ and (ii) the droplet impurities are almost half filled by setting fixed $\mu = 0$ for all droplet geometries. We emphasize that these two cases, which are equivalent in the conventional PAM on a square lattice, differ in our lattice geometry. In the former system, both the conduction and f electron densities are away from and can exceed half filling. In contrast, the latter system partially removes the charge fluctuations of the f electron, whose density is almost half filled while the conduction electron below half filling presents mostly the spatial density modulation. Because of the geometric frustration, the infamous Fermionic minus sign problem prevents us from the arbitrary choice of parameters for various droplet geometries. Therefore, to study a large enough lattice at low enough temperature with a manageable sign problem and computational cost, most results presented are for lattices with boundary length $L = 10$ sites such that the total number of sites is $3L^2 + 3L + 1 = 331$, which places constraints on the maximal possible number of impurity rings for a particular droplet ring distance n.

III. MAIN RESULTS

A. Local susceptibility

The key quantity throughout this paper is the local magnetic susceptibility, defined as

$$\chi_{ab}(\mathbf{r}) = \int_0^\beta d\tau \langle [n^a_{\mathbf{r}\uparrow}(\tau) - n^a_{\mathbf{r}\downarrow}(\tau)][n^b_{\mathbf{r}\uparrow}(0) - n^b_{\mathbf{r}\downarrow}(0)]\rangle, \quad (1)$$

where a and b denote the conduction and f electrons, respectively, and $\mathbf{r}$ is the location of the characteristic impurity along the red examination line in Fig. 1 on the $\mathbf{r}$th impurity ring so that the central impurity is at $\mathbf{r} = 0$. Note that this red examination line passes the lattice corner and the middle of the lattice boundary for A and B types of droplets, respectively. We remark that the reduced number of nearest impurities leads to differing spin correlations via Ruderman-Kittel-Kasuya-Yosida (RKKY) interaction and also different neighboring conduction electron seas so that the Kondo screening will largely affect the properties near the lattice boundary [10]. In some cases, the following results will cover the data near or at the boundary, although that is not our focus.

Figure 2 illustrates the evolution of the local f-electron susceptibility $\chi_{ff}(\mathbf{r})$ versus $\mathbf{r}$ for various A and B droplet geometries in systems with both $\rho = 1$ and $\mu = 0$, where we have simplified the label as $A/Bn \equiv A/B\{n : N_r\}$ for various cases of N_r. To access large enough droplets (especially for the $A1$ droplet), the temperature is chosen to be $T = t/10$, which is low enough to identify the essential properties presented here. The major features persist at a lower temperature $T = t/20$ with a smaller largest droplet size ($N_r = 5$ is practically the largest accessible $A1$ droplet due to the sign problem).

First, $\chi_{ff}(\mathbf{r})$ in systems with both $\rho = 1$ and $\mu = 0$ oscillates with increasing $\mathbf{r}$ for $A/B\{n : N_r > 2\}$ droplets (most clearly for the $A1$ droplet) before reaching the outermost ring, where this "regular" oscillation breaks down due to the lattice boundary effect mentioned before or a similar effect occurring at the droplet boundary [10]. Neglecting the droplets, e.g.,

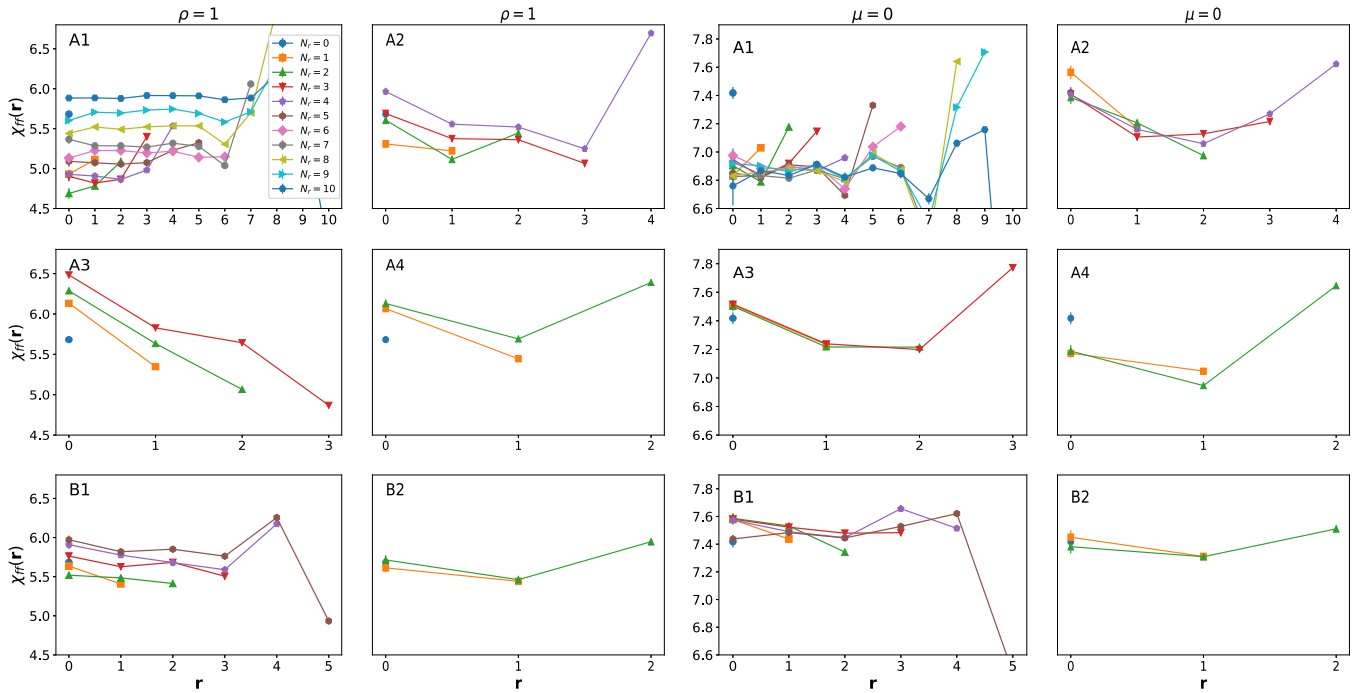

FIG. 2. Local f-electron susceptibility $\chi_{ff}(\mathbf{r})$ for various A and B droplet geometries in systems with both $\rho = 1$ and $\mu = 0$, where we have simplified the label as $A/Bn \equiv A/B\{n : N_r\}$ for various cases of N_r. $T = t/10$ is chosen to access large enough droplets (especially for $A1$ droplets).

$A\{1 : 9\}$ and $A\{1 : 10\}$, whose outermost ring approaches or locates at the lattice boundary, we note that $A1$'s outermost ring has an upturn of χ_{ff} while other droplets, e.g., $A\{2 : 3\}$ (the $\rho = 1$ system) and $A\{3 : 2\}$ (the $\mu = 0$ system), can have opposite trends. This complication stems from the density fluctuation (dominantly at the spatial region of the droplet boundary) of the system, which intertwines with the lattice and/or droplet boundary effects. In fact, as discussed in detail in Sec. III B, the local density fluctuation, which mostly comes from the conduction electrons especially in $\mu = 0$ systems, anticorrelates with the oscillations of $\chi_{ff}(\mathbf{r})$, which signifies the important role played by the charge degrees of freedom imposed by the inhomogeneous lattice.

Second, the oscillation of $\chi_{ff}(\mathbf{r})$ gradually diminishes with increasing N_r, namely, the droplet size, as most clearly shown for the $A1$ droplet of the $\rho = 1$ system. In other words, the droplet's central region becomes more and more homogeneous and coherent [26]. For other droplets with larger distance n between consecutive rings, we are limited by the lattice size to identify the diminishment of $\chi_{ff}(\mathbf{r})$.

Third, the weaker dependence of $\chi_{ff}(\mathbf{r})$ on N_r for B-type droplets compared with their A-type counterparts signifies the impact of the differing geometric arrangements of impurities, in particular, the distance between consecutive rings and the absence of nearest-neighbor impurities in B droplets. In the sense of the minimal hopping distance between the consecutive rings, the $B1$ ($B2$) droplet is more similar to the $A2$ ($A4$) droplet.

The major difference between systems with $\rho = 1$ and $\mu = 0$ is that $\chi_{ff}(\mathbf{r})$ in the latter system gradually saturates with N_r, while in the former system it continues to grow even for large N_r. This originates from the stronger charge effect in the globally half filled system $\rho = 1$. Taking the $A1$ droplet, for example, the site-dependent density keeps decreasing and approaches half filling upon increasing N_r, so that $\chi_{ff}(\mathbf{r})$ keeps growing in the former system, while the density saturates for a large enough N_r droplet in $\mu = 0$ systems (See Sec. III B). The strong charge effects can be suppressed to some extent by lowering the temperature, which has been verified at $T = t/20$ despite the limitation of accessing a smaller droplet size. At this point, we emphasize that the "full" suppression of charge effects requires pushing to a much lower temperature, which is difficult, if not impossible, in our DQMC simulations. The Kondo lattice model is more appropriate in this regard. All in all, the rich behavior of $\chi_{ff}(\mathbf{r})$ that is dependent on the droplet geometry indicates the possibility of artificial manipulation of the magnetic properties in a controllable manner.

One fascinating feature of $\chi_{ff}(\mathbf{r})$ is the strong dependence of $\chi_{ff}(\mathbf{r} = 0)$ at the central impurity on the droplet geometry. Figure 3 illustrates its evolution upon increasing N_r for various types of droplets. $\chi_{ff}(\mathbf{r} = 0)$ reflects the competition between interimpurity antiferromagnetic spin correlation and the surrounding impurity rings mediated via RKKY interaction and Kondo screening of the conduction electrons. Moreover, the charge fluctuations in our systems interplay with these two factors to complicate the whole picture. Figures 3(a) and 3(b) compare the behavior of $\chi_{ff}(\mathbf{r} = 0)$ between two types of systems at $T = t/10$, and Figs. 3(c) and 3(d) present the comparison at lower temperature $T = t/20$. For an A-type droplet with the smallest distance between rings, e.g., $n = 1$, $\chi_{ff}(\mathbf{r} = 0)$ decreases rapidly from its single-impurity value, and then Fig. 3(a) keeps growing in $\rho = 1$ systems, while Fig. 3(b) gradually saturates after an oscillating behavior in $\mu = 0$ systems with increasing N_r. As discussed before, this difference stems from the stronger charge effects in $\rho = 1$ systems, which can be partially suppressed at the lower

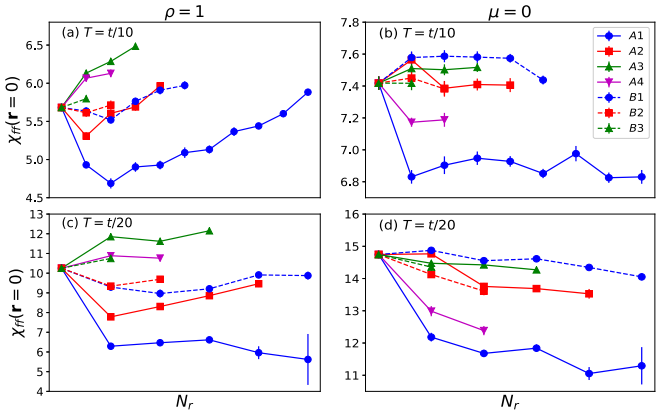

FIG. 3. Comparison of $\chi_{ff}(\mathbf{r}=0)$ at the central impurity as a function of the number of impurity rings N_r for various A and B droplets.

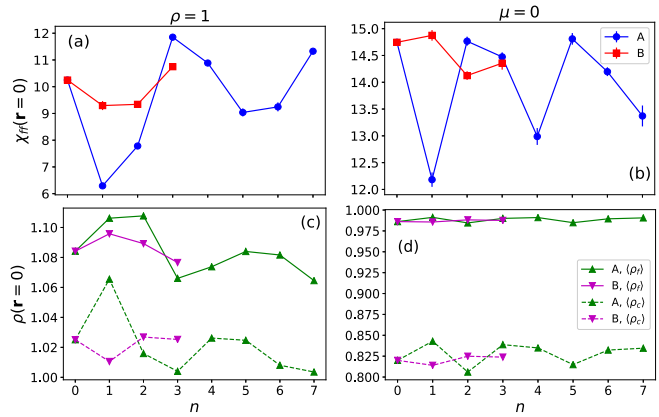

FIG. 4. (a) and (b) Comparison of $\chi_{ff}(\mathbf{r}=0)$ for droplets with a single impurity ring $N_r=1$ but varying distance n to the central impurity at $T=t/20$. (c) and (d) The local orbital-dependent occupancy at the central impurity anticorrelates with $\chi_{ff}(\mathbf{r}=0)$.

temperature $T=t/20$ shown in Fig. 3(c). This saturation similar to that reported for the KLM on a square lattice [10] can be attributed to the buildup of spin correlations induced from the neighboring droplet rings, which gives rise to the collectivelike screening of the central impurity. As pointed out in Fig. 2, $\chi_{ff}(\mathbf{r}=0)$ in B-type droplets has more moderate dependence on N_r. The moderate deviation from the single-impurity case implies the compensation between local Kondo, interimpurity spin correlation, and charge fluctuation effects. Unfortunately, it is impossible to access a much larger lattice and/or lower temperature to identify the saturation of all droplet geometries, especially the B type with a larger distance between the rings.

The most unusual feature in Fig. 3 due to the interplay between various intertwined effects manifests when increasing the distance n between impurity rings, where the fate of the decrease of $\chi_{ff}(\mathbf{r}=0)$ upon N_r is significantly modified. In fact, $\chi_{ff}(\mathbf{r}=0)$ can even be enhanced in $A3$, $A4$, and $B3$ droplets in $\rho=1$ and $A2$ and $B1$ droplets in $\mu=0$ systems [Figs. 3(a) and 3(b)], which persists at lower temperature $T=t/20$ [Figs. 3(c) and 3(d)]. As verified via the density profile in Sec. III B, this remarkable enhancement implies a significant charge redistribution due to the lattice inhomogeneity, which in turn results in the tunable magnetic susceptibility for a particular impurity embedded in a system.

To further understand the nontrivial dependence of the local magnetism upon the droplet geometry, we also explored $\chi_{ff}(\mathbf{r}=0)$ for droplets with a single impurity ring $N_r=1$ but varying distance n to the central impurity. As can be seen in Figs. 4(a) and 4(b), it oscillates periodically with n in both $\rho=1$ and $\mu=0$ systems, although the lattice size forbids accessing more oscillations for B-type droplets, which vividly depicts the tunability of the magnetic properties via modulation of the droplet geometry. The strong charge effect is illustrated in Figs. 4(c) and 4(d), which display the anticorrelation between the local density profile at the lattice center and $\chi_{ff}(\mathbf{r}=0)$. Although the charge fluctuation for the f electron can be partially suppressed by enforcing its nearly half filled occupancy via $\mu=0$, the density profile of the conduction electrons also plays an important role in determining the magnetic properties of the droplet.

B. Density fluctuation

Previously, we briefly mentioned that the local-density fluctuation anticorrelates with the oscillations of $\chi_{ff}(\mathbf{r})$. To provide more insights into the origin of the evolution of the magnetic properties with the droplet geometry, Fig. 5 illustrates the local occupancy of the droplet site $\rho_f(\mathbf{r})$ (solid lines) and conduction electrons $\rho_c(\mathbf{r})$ (dashed lines) in various systems, which shows this general anticorrelation vividly compared with Fig. 2. Specifically, taking the $A1$ droplet of the $\rho=1$ system, for example, the peak of $\rho_f(\mathbf{r}=0)$ versus N_r occurs at $N_r=2$, which coincides with the occurrence of the valley of $\chi_{ff}(\mathbf{r}=0)$ at the same N_r in Fig. 3(a).

The most important feature is the coincidence between $\chi_{ff}(\mathbf{r})$ and the closeness of $\rho_f(\mathbf{r})$ to unity. As $\rho_f(\mathbf{r})$ approaches unity with $\mathbf{r}$ and/or N_r, $\chi_{ff}(\mathbf{r})$ increases accordingly, which is a well-known consequence of the local magnetic moment associated with the forbidden double occupancy. This is clearly evidenced by the generally larger $\chi_{ff}(\mathbf{r})$ in $\mu=0$ systems because of the almost half filled droplet sites $\rho_f(\mathbf{r})\sim 1$. In other words, the evolution of $\chi_{ff}(\mathbf{r})$, especially the unusual enhancement of $\chi_{ff}(\mathbf{r}=0)$ with N_r (Fig. 3), presented in Sec. III A is strongly tied to the density redistribution via varying the droplet geometry. Apparently, this density fluctuation is closely related to the nonperiodicity of the lattice due to both the droplet geometry and the open boundary employed. Therefore, in essence, the possibility of artificial manipulation of the magnetic properties of the Anderson droplet in our current confined lattice system is realized via the potentially controllable density variation enforced by a finite boundary.

The flatness of the density profile for systems with large N_r implies that the inner region of the droplet becomes more and more homogeneous and coherent upon increasing N_r. For other droplets with larger distance n between consecutive rings, we are limited by the lattice size to identify the ultimate flatness of $\rho(\mathbf{r})$. The anomalous oscillations at the outermost ring are due to the lattice and/or droplet boundary effects similar to $\chi_{ff}(\mathbf{r})$. In addition, the general weaker dependence

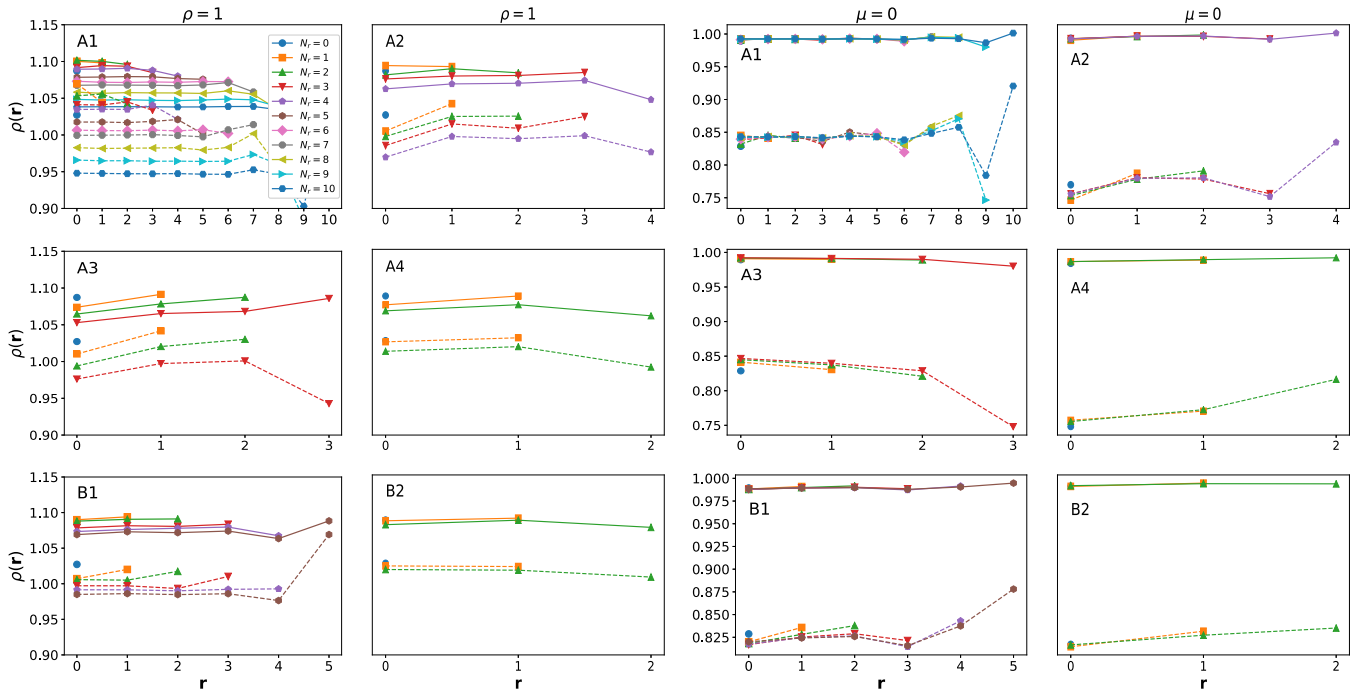

FIG. 5. Local orbital-resolved occupancy of droplet site $\rho_f(\mathbf{r})$ (solid lines) and conduction electrons $\rho_c(\mathbf{r})$ (dashed lines) in various systems at $T = t/10$. The general anticorrelation to $\chi_{ff}(\mathbf{r})$ shown in Fig. 2 is visible.

of $\rho(\mathbf{r})$ for B-type droplets on the droplet geometry matches the trend of $\chi_{ff}(\mathbf{r})$. In $\mu = 0$ systems, the density fluctuation mostly comes from the conduction electrons because the droplet sites are enforced to be nearly half filled. The major difference between systems with $\rho = 1$ and $\mu = 0$ lies in the saturation or not of $\rho(\mathbf{r})$ with increasing N_r. Apparently, the local-density saturation of the latter system mirrors the saturation of $\chi_{ff}(\mathbf{r})$.

C. Interorbital local susceptibility

It is not straightforward to compare our results to the latest exploration of Co adatoms on the Cu(111) surface [1] due to the intrinsic difficulty of extracting the local hybridization strength via the analytical continuation of the local interorbital Green's function. Instead, we illustrate the interorbital magnetic susceptibility $|\chi_{cf}(\mathbf{r})|$ that is found to largely anticorrelate with $\chi_{ff}(\mathbf{r})$, which naturally reflects the local competition between the Kondo screening and interimpurity spin correlation. Figure 6 displays the evolution of $|\chi_{cf}(\mathbf{r})|$ versus the location $\mathbf{r}$ for various droplets. Clearly, when $|\chi_{cf}(\mathbf{r})|$ increases (decreases) with $\mathbf{r}$ or N_r, the opposite trend occurs for $\chi_{ff}(\mathbf{r})$. The dominant feature is the generally weaker dependence of $|\chi_{cf}(\mathbf{r})|$ on N_r compared with $\chi_{ff}(\mathbf{r})$, which reflects the locality of $c - f$ hybridization, in contrast to the spatial character of interimpurity spin correlation manifested in $\chi_{ff}(\mathbf{r})$.

IV. PARAMETER DEPENDENCE OF MAGNETIC PROPERTIES

To provide more evidence of the robustness of our main results illustrated in Sec. III, in the following we discuss the effects of various parameters in more general settings. In addition, we will elaborate more upon the close relation between the local charge density and magnetic properties.

A. Finite-size effects

Finite-size effects are ubiquitous in lattice quantum Monte Carlo calculations. Typically, they are most serious when a question concerning long-range order is considered since, by definition, one is examining the asymptotic behavior at a large spatial separation. Our adoption of an open boundary condition for the lattice without the translational symmetry implies the potentially significant impact of the lattice size. Because the manifestation of the essential features, especially the enhancement of $\chi_{ff}(\mathbf{r} = 0)$ upon N_r, requires a large enough lattice, e.g., $L \geqslant 8$, while the computational cost limits us from simulating a much larger lattice, finite-size scaling is, by and large, meaningless in this context.

Therefore, here we provide only evidence that there are no qualitative changes for a larger lattice system with $L = 12$ compared with $L = 10$ adopted in Sec. III. Since, after all, the relevant physics is more or less local, e.g., the local repulsion for the f-conduction electron is strong coupling $U/t = 4.0$, we do not expect any significant modification of the local magnetic properties. Figure 7 confirms this expectation via the local susceptibility $\chi_{ff}(\mathbf{r} = 0)$ at the central impurity for $L = 12$ lattices at $T = t/10$.

Figures 7(a) and 7(b) compare the behavior of $\chi_{ff}(\mathbf{r} = 0)$ as a function of the number of impurity rings N_r between two types of systems. All the essential features presented in Fig. 3 remain in this larger lattice. In particular, the unusual feature of enhanced $\chi_{ff}(\mathbf{r} = 0)$ with N_r for some droplets persists. Furthermore, Figs. 7(c) and 7(d) display $\chi_{ff}(\mathbf{r} = 0)$ for

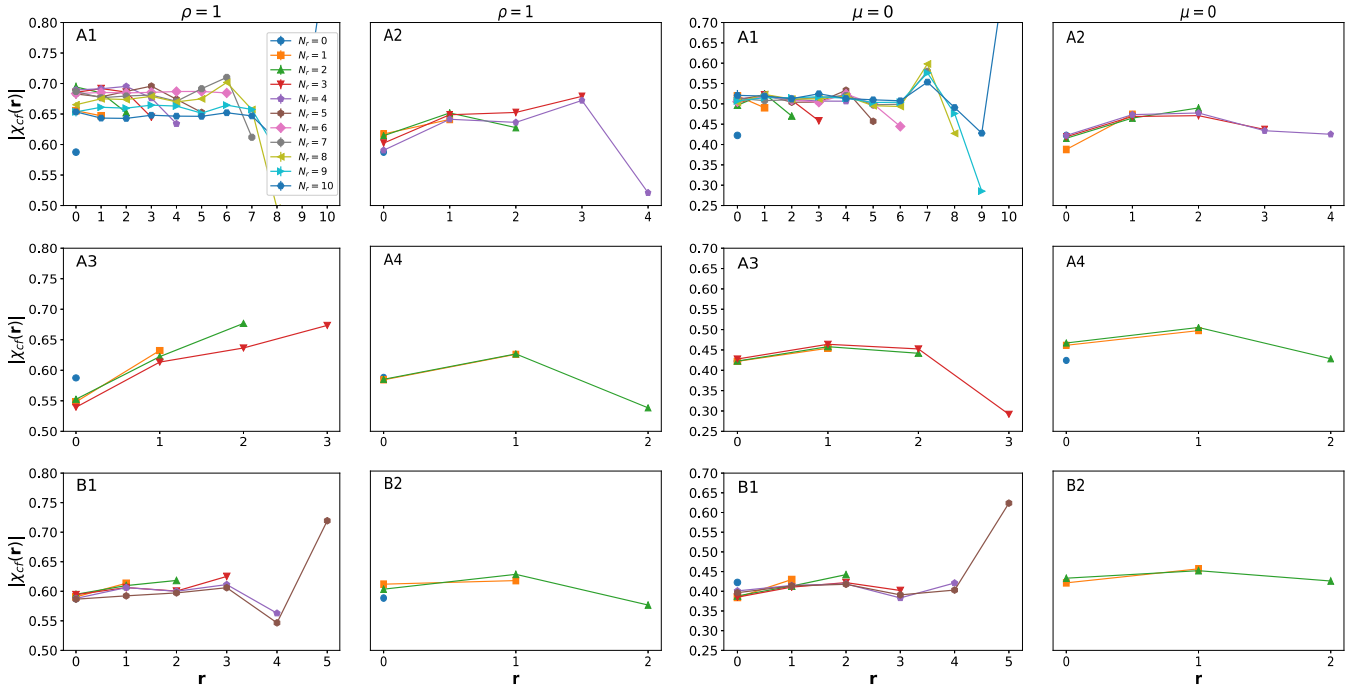

FIG. 6. Local interorbital susceptibility $|\chi_{cf}(\mathbf{r})|$ for various systems at $T = t/10$. The general weaker dependence on N_r and its anticorrelation to $\chi_{ff}(\mathbf{r})$ shown in Fig. 2 are visible.

droplets with a single impurity ring $N_r = 1$ as a function of its distance n to the central impurity. The oscillating behavior is reminiscent of that presented in Fig. 4. The robustness against the lattice size confirms our major conclusion of the tunability of the magnetic properties by the artificial arrangement of the droplet geometry.

B. Effects of hybridization strength V

In Sec. III, we fixed the $c - f$ hybridization strength as the characteristic $V/t = 1.0$. Because the Anderson lattice models describe the competition between interimpurity antiferromagnetic spin correlation mediated via RKKY interaction and the Kondo screening from conduction electrons, it is natural to ask about the impact of the $c - f$ hybridization strength. Similar to Fig. 7, Fig. 8 demonstrates the behavior of $\chi_{ff}(\mathbf{r} = 0)$ as a function of N_r for various droplets [Fig. 8(a)] and of n for droplets with a single impurity ring $N_r = 1$ [Fig. 8(b)] with varying distance n to the central impurity. Obviously, there is no qualitative modification of the tunable features of $\chi_{ff}(\mathbf{r} = 0)$ compared to those for smaller hybridization (Figs. 3 and 4) and for larger lattices (Fig. 7).

C. Effects of the chemical potential μ

In Sec. III, we focused on two special cases ($\rho = 1$ and $\mu = 0$) of orbital occupancies by tuning the chemical potential μ. Because the major difference of the Anderson-type models from the Kondo-type models is the involvement of the additional charge fluctuations in the determination of their physical properties, the role played by the chemical potential,

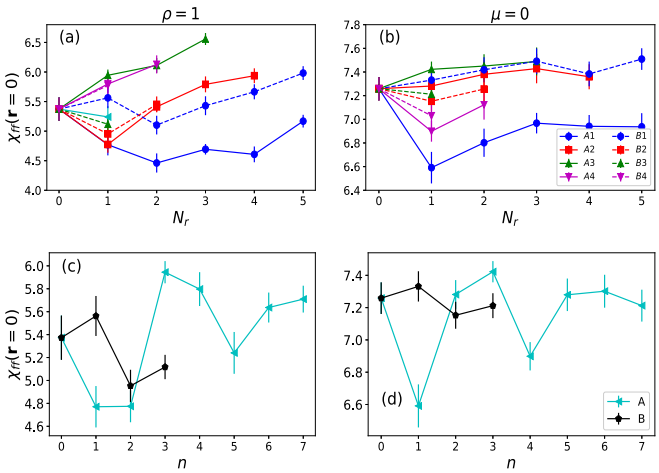

FIG. 7. Comparison of $\chi_{ff}(\mathbf{r} = 0)$ at the central impurity (a) and (b) as a function of the number of droplet rings N_r for various droplets and (c) and (d) as a function of ring distance n for droplets with a single droplet ring $N_r = 1$ in $L = 12$ lattices at $T = t/10$.

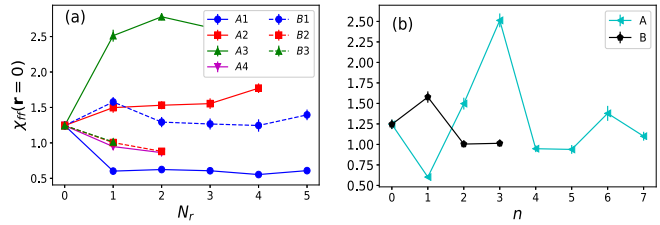

FIG. 8. $\chi_{ff}(\mathbf{r} = 0)$ at the central impurity (a) as a function of N_r for various droplets and (b) as a function of n for droplets with a single droplet ring $N_r = 1$ for $c - f$ hybridization strength $V/t = 2.0$ at $T = t/10$.

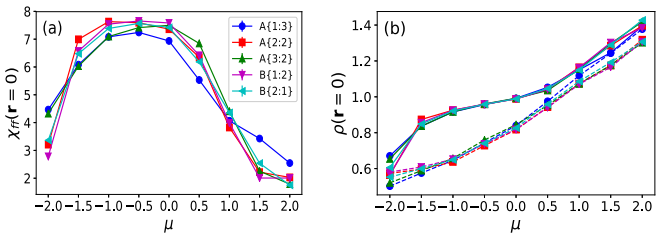

FIG. 9. (a) $\chi_{ff}(\mathbf{r}=0)$ and (b) the local orbital occupancy $\rho(\mathbf{r}=0)$ at the central impurity (solid lines for the droplet f orbital and dashed lines for conduction electrons) vs the chemical potential μ for $V/t=1.0$ in $L=10$ lattices at $T=t/10$.

namely, more general cases of orbital occupancies, is worth elaborating upon.

Figure 9(a) illustrates the evolution of $\chi_{ff}(\mathbf{r}=0)$ with μ for some characteristic droplets. Obviously, the dominant feature is the commonly broad peak at $\mu\sim-0.5$, which can be naturally accounted for by the local orbital occupancy $\rho(\mathbf{r}=0)$ (solid lines for the droplet f orbital and dashed lines for conduction electrons) shown in Fig. 9(b). Specifically, at $\mu\sim-0.5$, the features of both (i) the almost half filled occupancy of the droplet f orbital (solid lines) and (ii) the plateaulike evolutions with μ imply for the strongest magnetic local moment to induce the peak of local magnetic susceptibility. This further indicates the close relation between the local magnetic properties and charge density, as discussed in Sec. III.

D. Effects of Coulomb repulsion U

Our current work concentrates on the Anderson droplet model with the additional involvement of the charge degrees of freedom instead of the effective Kondo droplet model in the strong-coupling limit $U/t\to\infty$; it is worthwhile to discuss more about the role played by the Coulomb repulsion U.

Figure 10(a) displays the local magnetic moment of the droplet center $\langle m^2{}_f(\mathbf{r}=0)\rangle$ versus U for some characteristic droplets, and Fig. 10(b) shows the local orbital occupancy $\rho(\mathbf{r}=0)$ (solid lines for the droplet f orbital and dashed lines for conduction electrons). Here we adopt $\mu=0$ to facilitate

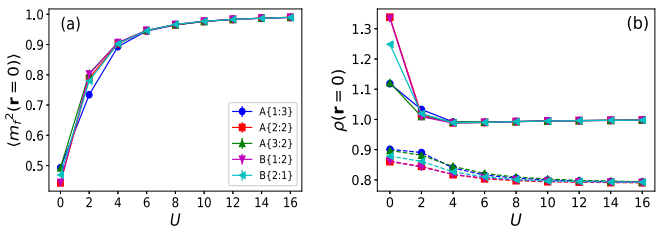

FIG. 10. (a) The local magnetic moment $\langle m^2{}_f(\mathbf{r}=0)\rangle$ of the droplet center and (b) the local orbital occupancy $\rho(\mathbf{r}=0)$ at the central impurity (solid lines for the droplet f orbital and dashed lines for conduction electrons) vs U for $V/t=1.0$ in $L=10$ lattices of $\mu=0$ systems at $T=t/10$.

the half-filled occupancy of the droplet center. Clearly, strong Coulomb repulsion saturates the local charge occupancy. As a result, the forbidden charge fluctuations and double occupancy at the half-filled droplet center lead to the enhanced and saturated local magnetic moment.

V. CONCLUSION

In conclusion, we have employed the numerically exact DQMC simulations in the framework of the Anderson droplet model to investigate the local magnetic properties associated with the hexagonal droplet embedded in a triangular lattice. We demonstrated the tunability of the magnetic properties by the evolution of local susceptibility with the droplet geometry for two types of systems with differing local orbital occupancy profiles. Our ADM has the intrinsic intertwined spin and charge degrees of freedom, whose fluctuations largely affect the local magnetic properties, although the charge fluctuation of the droplets can be partially suppressed by enforcing its nearly half filled occupancy.

The coincidence between the magnetic properties and the local charge occupancy is manifested by the unusual enhancement of $\chi_{ff}(\mathbf{r}=0)$ with N_r (Fig. 3) presented in Sec. III A, which is strongly tied to the density redistribution via varying the droplet geometry. This density fluctuation is, in turn, closely related to the nonperiodicity of the lattice due to both the droplet geometry and the open boundary employed. In essence, the possibility of artificial manipulation of the magnetic properties of the Anderson droplet in our current confined lattice system is realized via the potentially controllable density variation enforced by a finite boundary.

It is not straightforward to compare our results to the latest exploration of Co adatoms on the Cu(111) surface [1] due to (i) the intrinsic difficulty of extracting the local hybridization strength via the analytical continuation of the local interorbital Green's function, (ii) the strong charge effects in our ADM, and (III) the finite-size effect in contrast to the essentially infinitely large Cu(111) surface [1]. Further design of the lattice and/or droplet settings is required to perform an insightful direct comparison.

The natural extension of the present work is to investigate the Kondo droplet model [10] in the absence of the droplets' f-electron charge fluctuation and/or with more appropriate lattice band fillings. In addition, the Anderson version of Kondo holes in a droplet reported in the latest investigation deserves further exploration [1,27,28]. Although direct comparison with the recent progress on a quantum engineered Kondo lattice is not straightforward, our simulations complement the exploration of the novel artificial tunability of engineered confined lattice systems.

ACKNOWLEDGMENTS

This work was funded by the Stewart Blusson Quantum Matter Institute (SBQMI) of Canada. Computational resources were provided by SBQMI and Compute Canada.

[1] J. Figgins, L. S. Mattos, W. Mar, Y.-T. Chen, H. C. Manoharan, and D. K. Morr, arXiv:1902.04680.
[2] H. C. Manoharan, C. P. Lutz, and D. M. Eigler, Nature (London) **403**, 512 (2000).
[3] C. R. Moon, C. P. Lutz, and H. C. Manoharan, Nat. Phys. **4**, 454 (2008).
[4] C. F. Hirjibehedin, C. P. Lutz, and A. J. Heinrich, Science **312**, 1021 (2006).
[5] N. Tsukahara, S. Shiraki, S. Itou, N. Ohta, N. Takagi, and M. Kawai, Phys. Rev. Lett. **106**, 187201 (2011).
[6] K. K. Gomes, W. Mar, W. Ko, F. Guinea, and H. C. Manoharan, Nature (London) **483**, 306 (2012).
[7] M. R. Slot, T. S. Gardenier, P. H. Jacobse, G. C. P. van Miert, S. N. Kempkes, S. J. M. Zevenhuizen, C. M. Smith, D. Vanmaekelbergh, and I. Swart, Nat. Phys. **13**, 672 (2017).
[8] H. Kim, A. Palacio-Morales, T. Posske, L. Rózsa, K. Palotás, L. Szunyogh, M. Thorwart, and R. Wiesendanger, Sci. Adv. **4**, eaar5251 (2018).
[9] S. Wirth and F. Steglich, Nat. Rev. Mater. **1**, 16051 (2016).
[10] M. Raczkowski and F. F. Assaad, Phys. Rev. Lett. **122**, 097203 (2019).
[11] J. R. Schrieffer and P. A. Wolff, Phys. Rev. **149**, 491 (1966).
[12] P. Sinjukow and W. Nolting, Phys. Rev. B **65**, 212303 (2002).
[13] P. Sun and G. Kotliar, Phys. Rev. Lett. **95**, 016402 (2005).
[14] L. De Leo, M. Civelli, and G. Kotliar, Phys. Rev. B **77**, 075107 (2008).
[15] M. Jiang, N. J. Curro, and R. T. Scalettar, Phys. Rev. B **90**, 241109(R) (2014); M. Jiang and Y.-f. Yang, *ibid.* **95**, 235160 (2017).
[16] W. Wu and A.-M.-S. Tremblay, Phys. Rev. X **5**, 011019 (2015).
[17] A. Amaricci, G. Sordi, and M. J. Rozenberg, Phys. Rev. Lett. **101**, 146403 (2008).
[18] D. E. Logan, M. R. Galpin, and J. Mannouch, J. Phys.: Condens. Matter **28**, 455601 (2016).
[19] A. Amaricci, L. de' Medici, and M. Capone, Europhys. Lett. **118**, 17004 (2017).
[20] N. C. Costa, M. V. Araújo, J. P. Lima, T. Paiva, R. R. dos Santos, and R. T. Scalettar, Phys. Rev. B **97**, 085123 (2018).
[21] A. Benali, Z. J. Bai, N. J. Curro, and R. T. Scalettar, Phys. Rev. B **94**, 085132 (2016).
[22] T. Mendes-Santos, N. C. Costa, G. Batrouni, N. Curro, R. R. dos Santos, T. Paiva, and R. T. Scalettar, Phys. Rev. B **95**, 054419 (2017).
[23] M. W. Aulbach, F. F. Assaad, and M. Potthoff, Phys. Rev. B **92**, 235131 (2015).
[24] S. Hayami, M. Udagawa, and Y. Motome, J. Phys. Soc. Jpn. **81**, 103707 (2012).
[25] R. Blankenbecler, D. J. Scalapino, and R. L. Sugar, Phys. Rev. D **24**, 2278 (1981).
[26] The conditions for generating the coherent Kondo lattice behavior were investigated in Ref. [10], and that is currently not our focus in this work.
[27] J. Figgins and D. K. Morr, Phys. Rev. Lett. **107**, 066401 (2011).
[28] M. H. Hamidian, A. R. Schmidt, I. A. Firmo, M. P. Allan, P. Bradley, J. D. Garrett, T. J. Williams, G. M. Luke, Y. Dubi, A. V. Balatsky, and J. C. Davis, Proc. Natl. Acad. Sci. USA **108**, 18233 (2011).